Thermal conductivity measurements of laser crystals by infrared thermography. Application to Nd:doped crystals

Julien Didierjean, Emilie Hérault, François Balembois, Patrick Georges

Thermal conductivity measurements of laser crystals by infrared thermography. Application to Nd:doped crystals

Julien Didierjean, Emilie Herault, François Balembois, and Patrick Georges

Laboratoire Charles Fabry de l'Institut d'Optique,CNRS, Univ. Paris-Sud, Campus Polytechnique, RD 128, 91127 Palaiseau Cedex, France.
Julien.didierjean@institutoptique.fr

Abstract: We present a thermal conductivity measurement method for laser crystals based on thermal mapping of the crystal face by an infrared camera. Those measurements are performed under end-pumping of the laser crystal and during laser operation. The calculation of the fraction of pump power converted into heat is therefore simplified, and it is possible to link easily the temperature in the crystal to the thermal conductivity. We demonstrate the efficiency of this measurement method with a Nd:YAG crystal, before using it to compare Nd:YVO$_4$ and Nd:GdVO$_4$ crystals.

©2008 Optical Society of America

References and links

1. J. Parker, R. J. Jenkins, C. P. Butler, and G. L. Abbott, "Flash method of determining thermal diffusivity, heat capacity, and thermal conductivity," J. of Appl. Phys. **32**, 1679 (1961).
2. L. Pottier, "Micrometer scale visualization of thermal waves by photoreflectance microscopy," Appl. Phys. Lett. **64**, 1618 (1994).
3. A. Salazar, A. Sanchez-Lavega, and J. Fernandez, "Thermal diffusivity measurements in solids by the 'mirage' technique: Experimental results," J. of Appl. Phys. **69**, 1216 (1991).
4. J. F. Bisson, D. Fournier, M. Poulain, O. Lavigne, and R. Mévre, "Thermal conductivity of Yttria-Zirconia single crystals determined by spatially resolved infrared thermography," J. Am. Ceram. Soc. **83**, 1993-1998 (2000).
5. Y. Sato and T. Taira, "The studies of thermal conductivity in GdVO4, YVO4, and Y3Al5O12 measured by quasi-one-dimensional flash method," Opt. Express **14**, 10528-10536 (2006).
6. A. I. Zagumennyi, G. B. Lutts, P. A. Popov, N. N. Sirota, and I. A. Shcherbakov, "The thermal conductivity of YAG and YSAG laser crystals," Laser Phys. **3**, 1064-1065 (1993).
7. L. J. Qin, X. L. Meng, H. Y. Shen, B. C. Xu, L. X. Huang, H. R. Xia, P. Zhao, and G. Zheng, "Thermal conductivity and refractive indices of Nd:GdVO4 crystals," Cryst. Res. Technol. **38,** 793-797 (2003).
8. J.R. O'connor, "Unusual crystal field energy levels and efficient laser properties of YVO4:Nd3+," Appl. Phys. Lett. **9**, 407.
9. A. I. Zagumennyi, V. G. Ostroumov, I. A. Shcherbakov, T. Jensen, J. P. Meyen, and G. Huber, "The Nd:GdVO4 crystal, a new material for diode-pumped lasers," Sov. Quantum Electron. **22**, 1071-1072 (1992).
10. B. H. T. Chai, G. Loutts, J. Lefaucheur, X. X. Zhang, P. Hong, M. Bass, I. A. Shcherbakov, and A. I. Zagumennyi, "Comparison of laser performance of Nd-doped YVO$_4$, GdVO$_4$, Ca$_5$(PO$_4$)$_3$F, Sr$_5$(PO$_4$)$_3$F, and Sr$_5$(VO$_4$)$_3$F," Proceeding OSA ASSL 1994, **20**, 41 (1994).
11. C. Kränkel, *et al.*, "Continuous wave laser operation of Yb3+:GdVO4," Appl. Phys. B **79**, 543-546 (2004).
12. P. A. Studenikin, A. I. Zagumennyi, Yu. D. Zavartsev, P. A. Popov, I. A. Shcherbakov, "GdVO$_4$ as a new medium for solid-state lasers: some optical and thermal properties of crystals doped with Cd^{3+}, Tm^{3+}, and Er^{3+} ions, , Quantum Electron. **25**, 1162 (1995).
13. W. Koechner, "*Solid State Laser Engineering,*" 5th version, (Springer, 1999).
14. A. Cousins, "Temperature and thermal stress scaling in finite-length end-pumped laser rods," IEEE J. Quantum Electron. **28**, 1057 (1992).
15. S. Chenais, F. Druon, S. Forget, and F. Balembois, "On thermal effects in solid-state lasers: The case of ytterbium doped materials," Prog. Quantum Electron. **30**, 89-153 (2006).

16. T. Y. Fan, "Heat Generation in Nd:YAG and Yb:YAG," J. of Quantum Electron. **29**, 1457-1459 (1993).
17. I. Shoji, T. Taira, T. Taira, and A. Ikesue, "Thermally-induced-birefringence effects of highly Nd3+-doped Y3Al5O12 ceramic lasers," Opt. Mater. **29**, 1271-1276 (2007).
18. R. Gaume, B. Viana, and D. Vivien, "A simple model for the prediction of thermal conductivity in pure and doped insulating crystals," Appl. Phys. Lett. **83**, 1355-1357 (2003).
19. T. Ogawa, Y. Urata, S. Wada, K. Onodera, H. Machida, H. Sagae, M. Higuch, and K. Kodaira, "879nm-LD-pumped Nd:GdVO4 laser and its thermal property, " OSA Trends in Optics and Photonics **94**, 293-297 (2004).
20. A. I. Zagumennyi, V. A. Mikhailov, V. I. Vlasov, A. A. Sirotkin, V. I. Podreshetnikov, Yu. L. Kalachev, Yu. D. Zavartsev, S. A. Kutovoi, and I. A. Shcherbakov, "Diode-pumped lasers based on GdVO$_4$ crystal," Laser Phys. **13**, 311 (2003).

1. Introduction

Diode-pumped solid state lasers have been largely developed during the past years, and they are appreciated for their efficiency and output mode quality, especially in end-pumped configuration. Nevertheless, usual bulk crystals are limited in output power by thermal issues, due to a relatively bad heat management. This issue leads to thermal beam distortion, induced birefringence and even fracture of the crystals. All those problems show the importance of the thermo-mechanical properties of the laser crystals. One of the key parameter is the thermal conductivity Kc. This parameter is usually determined indirectly, through thermal diffusivity measurements. The thermal conductivity can be then calculated by the relation $Kc = \alpha_T . \rho . Cp$ (α_T is the thermal diffusivity, ρ is the density and Cp is the specific heat). The most common method to measure this diffusivity is the Flash method presented by Parker, *et al.*[1]. In this setup, the material is heated by a flash lamp, and the heat diffusion to the back surface is recorded. The diffusivity can then be deduced from the evolution of the temperature versus time. Many variations of this method were demonstrated and applied to laser crystals. The detection of the heat diffusion can be made by photoreflectance microscopy [2], deflection of a probe beam (Mirage) [3], interferential methods, or infrared thermography [4]. The flash lamp can also be replaced by a short laser pulse, to be sure that the heating pulse width is smaller than the diffusion time through the sample. Those methods seem to give reliable thermal conductivity results in many materials, but they have several drawbacks. The determination of the conductivity is indirect, depending on diffusivity, heat capacity and density of the material. The deposition of a thin layer (Carbon or metal) for absorption of the heating pulse is often required. For accurate measurements, the sample front face must be heated uniformly, there should be no heat loss to the external environment, and the heating pulse must be short compared to the rising time of the temperature inside the sample. For flash sources emitting in the near IR (below 5µm), the flash method is more difficult to achieve with reliable results because many laser crystals are transparent from visible to middle infrared, and the flash light may be directly transmitted in the transparent media to the back face, where the heat detection is done. This effect leads to overestimation of the diffusivity, as explained in [5].

Those issues lead to large dispersion of the conductivity values reported for some laser crystals in publications. The well established Nd:YAG crystal is known for its good thermal conductivity (Kc = 10.7 W/(m.K) for 1% at. in Nd^{3+} [7]) but during the last past years it was often replaced by other crystals with better laser properties like Nd:YVO$_4$ [8] and Nd:GdVO$_4$ [9]. Those crystals show high emission and absorption cross sections, but their thermal conductivities are subject to discussion. In the literature, one can find conductivity values ranging from 5.1 W/(m.K) [10] to 8.9 W/(m.K) [5] for a-cut Nd:YVO$_4$ crystals, and from 6.5 W/(m.K) [11] to 11.8 W/(m.K) [12] for a-cut Nd:GdVO$_4$ crystals. Many publications, like Qin, *et al.* [7], show a clear advantage of the GdVO$_4$ lattice on the YVO$_4$ one, whereas, Sato and Taira [5] recently published results showing that for doping concentration below 1% at. in Nd^{3+}, the Nd:YVO$_4$ has a higher conductivity. We think that another method of thermal conductivity measurements could be of great interest to complete those results. In this paper,

we present a new method to measure the thermal conductivity, by direct thermal mapping of the crystals under laser operation. In section 2 we will deal with the theoretical principle of the method. Section 3 presents the experimental setup. In section 4 we validate our method by measurement on a Nd:YAG sample. Section 5 presents measurements on Nd:YVO$_4$ and Nd:GdVO$_4$ crystals.

2. Principle of thermal conductivity measurement by thermal mapping under laser operation

For analytical calculations, we will use a model that requires three hypotheses:
1) The heat load repartition has a radial symmetry. This is justified in fiber-coupled laser diode pumping.
2) The thermal conductivity is a scalar: it does not depend on the crystal axis. This is a strong approximation, as many laser crystals are not isotropic, and therefore can have different thermo-mechanical properties along their different axis.
3) The heat evacuation is radial. To check this hypothesis, we define the heat transfer coefficient H between two media, thanks to Eq. (1).

$$-K_c \frac{dT}{dn} = H.(T_{crystal\_edge} - T_{mount})$$ (1)

Where K_c is the thermal conductivity, T is the temperature, and n is the coordinate normal to the interface. For a laser crystal placed in a copper mount, H was estimated around 1 W.cm^{-2}.K^{-1}[13]. For the faces of the crystal in contact with air, the heat transfer coefficient was estimated to be approximately 10^{-3} W.cm^{-2}.K^{-1}[14]. Consequently, the hypothesis that the heat flow is mainly radial seems fully justified in end-pumped configuration for a crystal inserted in an appropriate copper mount (see Fig. 1).

Thanks to the general heat equation, and assuming those hypotheses are true, the temperature gradient between the center and the edge of an-end-pumped laser rod of diameter r_0 is given by the expression below [15]:

$$T(r,z) - T(r_0,z) = -\frac{\eta_h}{4\pi.Kc} \frac{dP}{dz}(z).f(r,z)$$ (2)

Where η_h is the fractional thermal loading, dP/dz (z) represents evolution of the pump power along the z axis, and f(r,z) is a geometrical function depending on the pump geometry. Assuming a flattop radial profile for the pump beam, this function can be described by Eq. (3) :

$$\begin{cases} f(r,z) = \ln\left(\frac{r_0^2}{w_p^2(z)}\right) + 1 - \frac{r^2}{w_p^2(z)} & \text{if } r < w_p(z) \\ \\ f(r,z) = \ln\left(\frac{r_0^2}{r^2}\right) & \text{if } r > w_p(z) \end{cases}$$ (3)

Where $w_p(z)$ represents the waist radius of the pump beam along the z axis. Figure 1 presents the general scheme for an end-pumped crystal with the hypothesis mentionned before.
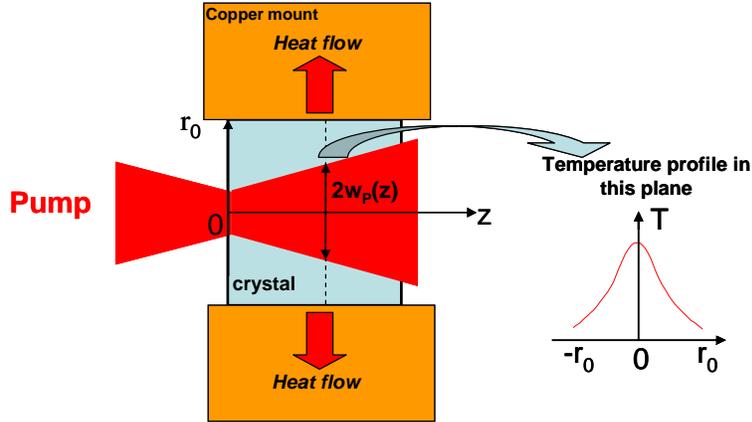
Fig. 1. Basic scheme for an end-pumped laser crystal

2.1 Determination of dP/dz

The absorption of the pump intensity I_p inside the crystal can be described by Eq. (4), assuming there is no reabsorption at the laser wavelength. In our case, this hypothesis is fully justified for the 1-µm transition in Nd^{3+} as it is a 4-level laser system :

$$\frac{dI_p}{dz} = -\alpha.I_p = -\frac{\alpha_{NS}(1+\frac{I}{I_{l_{sat}}})}{1+\frac{I_p}{I_{p_{sat}}}+\frac{I}{I_{l_{sat}}}}.I_p \tag{4}$$

Where α is the absorption coefficient, I is the intracavity laser power, α_{NS} is the unsaturated absorption coefficient at the pump wavelength, and the saturation intensity of the pump (I_{psat}) and the laser (I_{lsat}) are defined as :

$$I_{p_{sat}} = \frac{1}{(\sigma_{abs}(\lambda_p) + \sigma_{em}(\lambda_p)).\tau} \tag{5}$$

$$I_{l_{sat}} = \frac{1}{\sigma_{em}(\lambda_l).\tau} \tag{6}$$

Where $\sigma_{abs}(\lambda)$ and $\sigma_{em}(\lambda)$ are the absorption and stimulated emission cross sections, respectively. The evolution of the pump intensity $I_p(z)$ can therefore be calculated numerically, by dividing the crystal in small slices of thickness dz. It is then possible to calculate the dP/dz factor with a good accuracy, taking into account bleaching effects. However, one can remark that for a high intracavity laser intensity, the absorption is desaturated by the laser effect and the absorption coefficient α becomes close to α_{NS}. We calculated [thanks to Eq. (4)] the evolution of the absorption coefficient along the z-axis of a 1% at. doped Nd:YAG crystal under the experimental conditions described in section 4, with and without laser effect, to show that the absorption is clearly desaturated by the intracavity laser intensity. The result is shown on Fig. 2.
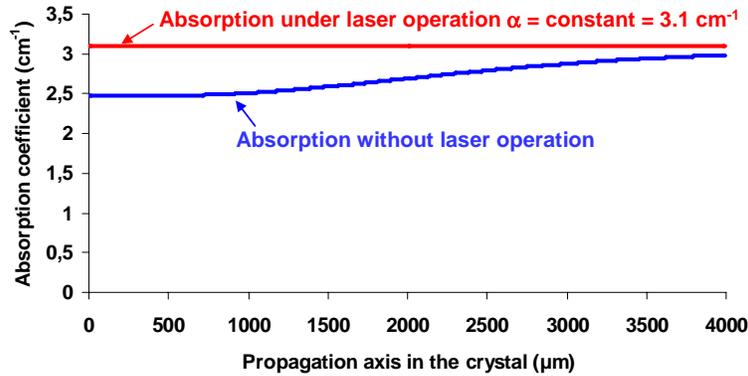
Fig. 2. Calculated absorption coefficient along the z-axis of the 1% at. doped Nd:YAG crystal, in the experimental conditions, with and without laser emission. The pump power is 25 W, the intracavity laser power is 140 W. The effect of bleaching is clearly visible without the laser, but disappears under laser operation.

The same calculations were carried out for the other crystals used experimentally, with similar results. Therefore it is possible to consider that $\alpha = \alpha_{NS}$ = constant under laser effect in our experimental conditions. It is then possible to simply write :

$$\frac{dI_p}{dz} = -\alpha_{NS} . I_p \tag{7}$$

In this case, the absorption of the pump power in the crystal can be calculated very simply, and one can write, in the entrance plane of the crystal :

$$\frac{dP}{dz}_{(z=0)} = -\alpha_{NS} . P_0 \tag{8}$$

Where P_0 is the incident pump power.

2.2 Estimation of the η_h parameter

The fractionnal thermal loading η_h is defined as the fraction of absorbed pump power converted into heat. This fraction is usually hard to determinate properly, since it depends on many parameters and because it is related to a large range of different heating mechanisms. Fan gives the following expression of η_h [16]:

$$\eta_h = 1 - \eta_p [(1-\eta_l)\eta_r(\lambda_p / \lambda_f) + \eta_l(\lambda_p / \lambda_l)] \tag{9}$$

Where η_p is the pump quantum efficiency, η_l is the laser extraction efficiency, corresponding to the fraction of ions of the upper laser level extracted by stimulated emission (= 0 without laser operation), and η_r is the radiative quantum efficiency of the upper metastable level. λ_p is the pump wavelength, λ_f is the average fluorescence wavelength, and λ_l is the laser wavelength.

In Nd doped crystals, the absorption transition around 0.8 µm is well known for its large cross section. In such a transition, in good quality laser crystals, η_p can be considered to be close to unity [15]. In all our calculations we will therefore consider $\eta_p \sim 1$.

Without laser extraction, $\eta_l = 0$. In this case, it is difficult to give an accurate value of the fractionnal thermal load. The lack of an efficient laser extraction leads to accumulation of ions in the excited level, enhancing parasitic heating effects like cross-relaxations, upconversion,

etc. Those effects are difficult to evaluate with good precision and depend on the experimental conditions, and consqently η_h is uneasy to determinate.

In laser operation, the laser extraction efficiency, η_l can be estimated through Eq. (10) [15], with the approximation that there is no reabsorption at the laser wavelength.

$$\eta_l = \frac{\sigma_e I}{\sigma_e I + 1/(\eta_r . \tau)} \tag{10}$$

In this expression, σ_e is the emission cross section at the laser wavelength, I is the intracavity laser power, τ is the lifetime of the active ion. One can remark that with high intracavity laser power, η_l tends to become close to unity. This is equivalent to saying that every ion in the excited state will contribute to stimulated emission. In this case, the fractional thermal load η_h is independent of the radiative quantum efficiency η_r, and η_h is simply equal to the quantum defect:

$$\eta_h = 1 - \lambda_p / \lambda_l \tag{11}$$

To achieve this, it is necessary to make measurements under efficient laser operation, in a low-loss cavity to maximise the intracavity power. In Nd-doped crystals, the four-level transition around 1.06µm is well known for its high efficiency, and could therefore be used to achieve $\eta_l = 1$.
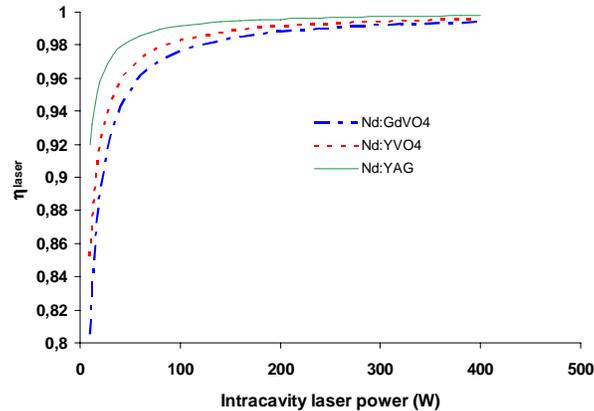

Fig. 3. Evolution of the laser extraction efficiency with the intracavity laser power.

The theoretical curves of η_l versus intracavity laser power are plotted in Fig. 3 for typical 1% at. doped Nd:YAG, Nd:YVO$_4$ and Nd:GdVO$_4$ crystals, for a laser waist of 400 µm diameter. For intracavity laser power above 200 W, it is a very good approximation to consider the laser extraction efficiency close to unity at the center of the laser mode (r = 0), where the intensity is maximum. Nethertheless, as the laser beam is Gaussian, it is important to check if η_l remains close to unity in all the area where the pump is absorbed and in particular in a plane perpendicular to the z axis. For that purpose, we plotted in Fig. 4 the evolution of the η_l function versus the radial coordinate r, assuming a Gaussian laser mode, a supergaussian pump mode corresponding to our experimental setup (cf. section 3) and using formula (10).
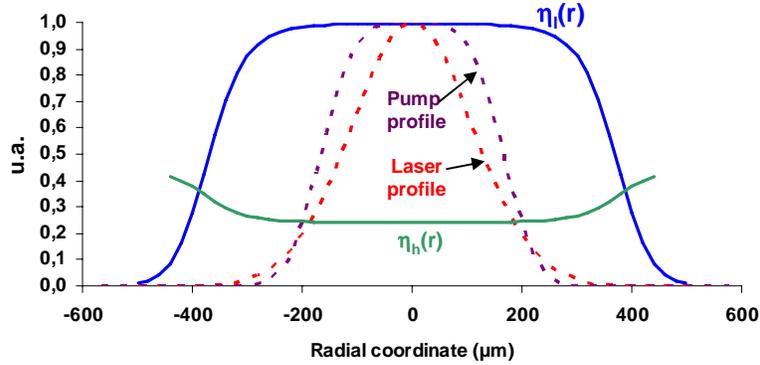
Fig. 4. Radial evolution of η_l and η_h parameters in a Nd:YVO$_4$ crystal with a 300 W intracavity laser power.

One can see that the η_l value remains very close to unity in all the pumped region if the intracavity laser power is high enough. In this case, considering pumping at 808 nm and laser effect at 1064 nm, Eq. (11) gives $\eta_h = 0.24$ in laser operation within all the pumped region of the crystal. Such fractionnal thermal load was measured experimentally by Taira and al. for a 1% at. doped Nd:YAG crystal in laser operation [17].

2.3 Determination of Kc

For experimental reasons (see section 2), it is only possible to measure the temperature map of the crystal faces. We chose to measure the temperature on the pumped face located in the plane z = 0 (see Fig. 1). In this plane, we can establish, thanks to Eqs. (2), (8) and (11), that:

$$T(r, z = 0) - T(r_0, z = 0) = \frac{1}{Kc} \cdot \frac{1}{4\pi} (1 - \frac{\lambda_p}{\lambda_l}) \cdot (\alpha . P_0) \cdot f(r, z = 0) \tag{12}$$

This formula is true all along the radius r of the crystal. T(r,z=0) - T(r$_0$,z=0) will be measured by IR thermography. Kc is the only unknown parameter, all the others parameters can be calculated with values corresponding to the experimental setup. Therefore, Kc can be adjusted to fit the experimental results to the calculations.

In cases where the formula (12) is not applicable (for example for anisotropic crystals), we will rely on finite element analysis (FEA) to fit the measured temperature profiles (see section 5).

3. Experimental setup

The infrared measurements were carried out in the 8-12 µm range because the measured temperatures correspond to IR peak emission in this wavelength band and because laser crystals are typically not transparent in this spectral domain. Consequently, we are only able to measure the temperature map on the crystal faces. The pumped face, receiving all the pump power, is the most interesting for our measurements. For that purpose, we designed the experimental setup presented in Fig. 5.

We used a fiber-coupled laser diode from LIMO (Germany) with a maximum output power of 60 W at 808 nm. The core diameter of the fiber is 400 µm. For laser operation at 1064 nm, we used a simple two mirrors cavity between a plano-concave mirror M$_2$ and a plane mirror M$_1$ (which can be one face of the crystal with a high reflection (HR) coating). To ensure $\eta_l = 1$ in formula (10), the laser must operate far above threshold, with high intracavity power. For that purpose, we used high reflectivity mirrors instead of output couplers. The laser cavities were designed by ABCD matrix simulations to fit the laser mode with the size of

the pumped area. We used different crystal mounts and different laser cavities and we checked that the experimental results were independent from the experimental parameters.

The laser crystals are placed inside a water-cooled copper mount. The thermal contact between the crystal and the copper is achieved by using a thin layer of thermal grease. The pump beam is reflected with a 90° angle by a ZnSe plate with high reflection coating at 1µm and high transmission in the 8-12 µm spectral range. The plate has a reflectivity of 97.5% at 1064 nm and 94% at 808 nm. Thanks to this dichroïc plate, it is possible to separate the pump beam from the thermal emission of the crystal. For thermal imaging, a Germanium aberration-free objective with NA 0.7 and focal length 50 mm is used. The detector is an infrared camera AGEMA 570 from *Flir system Inc.* operating in the 8-12 µm range. The detection matrix is composed of 320 x 240 microbolometers working at room temperature. The resolution of the image is limited by the size of the microbolometers (62 x 62 μm^2) and the magnification of the total thermal imaging system is close to unity. Therefore, a 3 x 3 mm^2 crystal face will be imaged in approximately 50 x 50 pixels.
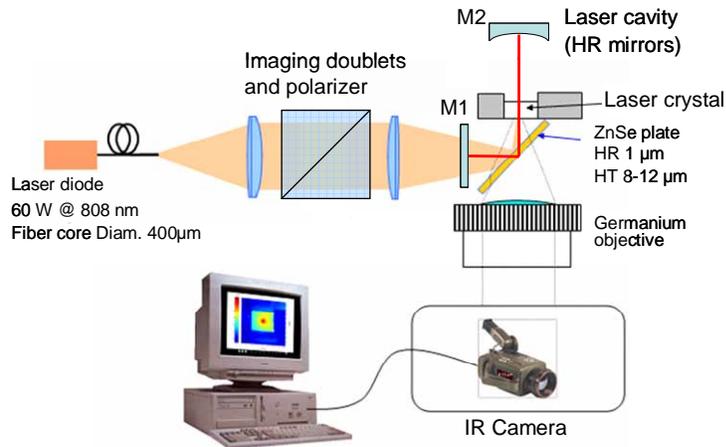

Fig. 5. Experimental setup for thermal conductivity measurement. The polarizer is only used for anisotropic crystals.

The emission of a material in the IR band depends on its temperature but also on its emissivity. An ideal blackbody has an emissivity of unity, but the laser crystals cannot be considered as such. Therefore, we need to calibrate the IR detector to know the exact relation between the temperature measured by the camera and the real temperature on the pumped face. This calibration depends on many parameters: the crystal emissivity, the coatings, and all the environment around experimental setup, which also emits in the thermal range. To make an accurate calibration, the crystal within its mount is heated uniformly by a Peltier element, without diode pumping. Thanks to a temperature probe placed inside the copper mount, we can measure the real temperature of the mount, which is equal to the temperature of the crystal after a thermalisation time. This real temperature was plotted versus the temperature measured on the crystal face by the IR camera, for a temperature ranging from 20°C to 100°C. An example of calibration curve for a Nd:YAG crystal is plotted on Fig. 6. The calibration curves observed are always found to be linear. By applying the appropriate linear transformation to the measured temperature, it is then easy to obtain the real temperature value.
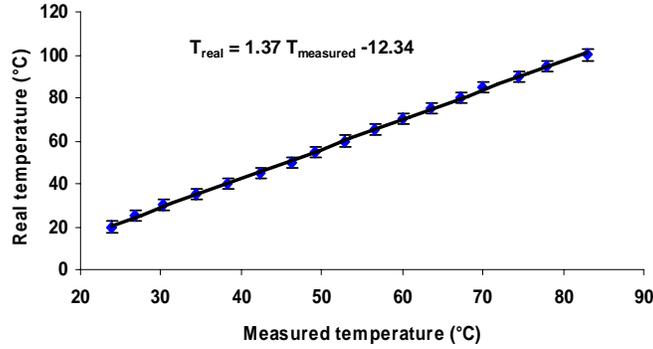
Fig. 6. Calibration curve of a Nd:YAG crystal

3.1 Measurement of the pump beam profile

As we need to know the pump profile in order to calculate the heat deposition inside the laser crystals, we made measurements of the radial pump profile at the focal point, with a beam analyzer. The results are shown on Fig. 7.
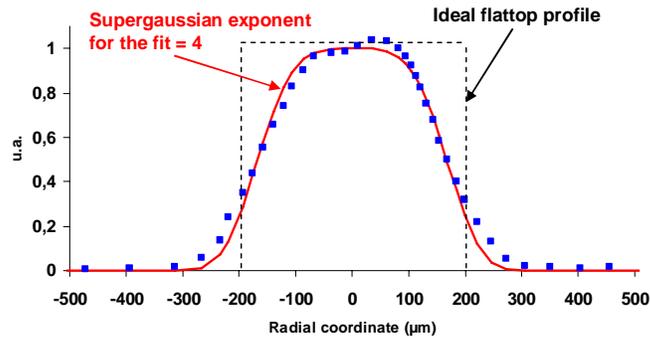

Fig. 7. Measurement and fit by a supergaussian function of the radial pump profile at the focalization point, for a magnification of 1 of the output of the diode by two doublets.

The measured profile is best fitted by a supergaussian function than by a flattop profile. This fit function was used as the input pump profile for the results given in Fig. 4 and for all the FEA simulations. The results given by analytical calculations (assuming a flattop pump profile) and the FEA simulations (using the fit function for the pump profile) are presented for the case of the Nd:YAG crystal in section 4 (see Fig. 8). The axial evolution of the pump radius, $w_p(z)$, can be described by Eq. (13):

$$w_p^2(z) = w_{p0}^2 + \frac{(M_p^2.\lambda_p)^2}{\pi^2.w_{p0}^2}.(z - z_0)^2 \qquad (13)$$

Where w_{p0} is the radius of the pump beam measured at the focal point, M_p^2 is the M^2 factor of the pump beam, and z_0 is the longitudinal coordinate of the focal point. We measured w_{p0} = 220 µm for a magnification of 1 of the output of the diode by two doublets, and w_{p0} = 170 µm for a magnification of 0.75. M_p^2 was measured to be approximately 150. The pump was focused close to the input face of the crystal (z_0 = 0) (cf. Fig. 1).

3.2 Evaluation of the measurements accuracy

From expression (12), we can calculate that :

$$\frac{dKc}{Kc} = \sqrt{\left(\frac{d(\Delta T)}{\Delta T}\right)^2 + \left(\frac{d(\alpha P_0)}{\alpha P_0}\right)^2 + \left(\frac{df(r,z)}{f(r,z)}\right)^2} \qquad (14)$$

Systematical errors on ΔT measurements come from error on the calibration curve and from error on the IR camera measurements. The precision of the thermocouple used for the calibration is below 2%, the precision on the temperature measurement of the IR camera is below 2.5%, according to their technical specifications. This gives a total error on the temperature gradient measurement of approximately 3%. The precision of the power detector used for the absorption measurements is specified at 2.5%, so the total precision on the αP_0 parameter is 3.5%. The function $f(r,z)$ mainly depends on the measurement of ω_p, which is the radius of the pump spot [see Eq. (3)]. This radius, if measured with a high sensibility camera, can be known with a precision around 2%, resulting in a precision of $f(r,z)$ estimated around 1% by error propagation calculations.

Determination of Kc is related to the validity of Eq. (12). We compared it with FEA analysis and found a good agreement, with a difference below 2% (see Fig. 8). Those calculations result in a maximum systematical error of 6% on the conductivity measurements. This error is based on the temperature measurement on only one point (r, z=0) of the crystal. Practically, we make the fit between experimental and analytical results on more than 40 experimental points on each profile, by a least square algorithm.

4. Thermal conductivity measurements on Nd:YAG

We used a 1% at. doped Nd:YAG crystal, square section 5x5 mm^2, length 4 mm. The faces of the crystal received anti-reflection coatings at 808 nm and 1064 nm. The pump power incident on the crystal is $P_0 = 24$ W. The 400 µm output fiber of the laser diode is imaged in the crystal with a magnification of 1, by two doublets. The unsaturated absorption coefficient of the crystal is measured to be $\alpha = 3.1$ cm^{-1}. Laser operation at 1064 nm is achieved in a two mirror cavity. M1 is a flat dichroïc mirror and M2 is a concave mirror with radius of curvature 300 mm. Both are highly reflective at 1064 nm. The laser threshold is very low, around 1W of pump power. This confirms that the cavity has low losses. By measuring the power leak of the ZnSe plate, we estimated the laser power intracavity to 140 W. By using formula (10) in this configuration, we found $\eta_l = 0.998$ (see Fig. 3).
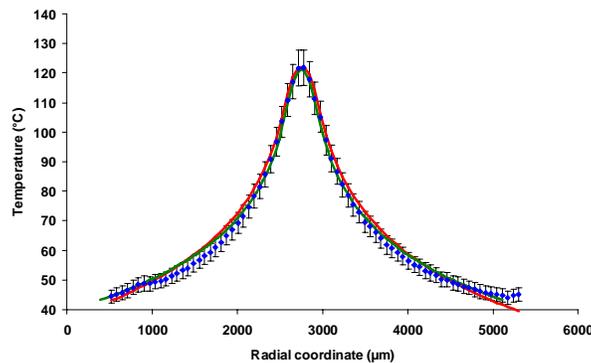

Fig. 8. Experimental (blue), theoretical (red) and simulated (green) radial temperature profiles of the pumped face of the Nd:YAG crystal at 24 W. The theoretical curve is calculated through Eq. (8), the simulated curve is calculated by FEA.

The experimental temperature profile is presented in Fig. 8, with the best analytical fit and the best FEA fit. The best analytical fit is obtained for a thermal conductivity value of Kc = 10.7 W/(m.K), the best FEA fit is obtained for Kc = 10.5 W/(m.K) (Details about the fit process by FEA analysis are presented in section 5). We observe very good agreement between the three profiles, validating the analytical Eq. (12).The accuracy is estimated to be +/- 0.6 W/(m.K) thanks to the study of section II. Repeatability measurements are shown on Fig. 9 and for 8 measurements, the standard deviation of the conductivity value is about 2%.
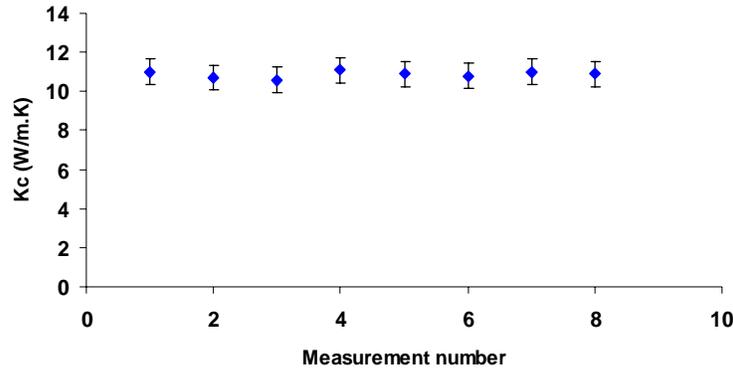

Fig. 9. Repetability of the thermal conductivity measurements for a Nd:YAG crystal

The results are in very good agreement with the tabulated value of this well known crystal [6-7]. It validates the method of thermal conductivity measurements by IR cartography under laser operation. With this new method, we are able to measure the thermal conductivity of laser crystals under pumping conditions. The results given by this method can also bring new answers when thermal conductivity measurements by other classical methods disagree.

5. Thermal conductivity measurements on Nd:YVO$_4$ and Nd:GdVO$_4$ crystals

Nd:YVO$_4$ and Nd:GdVO$_4$ are uniaxial crystals, with different conductivities on their a and c axes. In anisotropic crystals with thermal conductivity strongly depending on the axis, the temperature map doesn't have radial symmetry, and formula (2) is no more applicable. More precisely, the analytical geometrical function f(r,z) defined by (3) is not representative of the heat repartition in the crystal. If we want to make measurements on such crystals, it is possible to bypass the approximations made to demonstrate formula (2) and fit temperature measurements with numerical simulations, by Finite Element Analysis. Those simulations codes, by calculating the heat transfer between one small element and every neighbor element, can take into account the possible anisotropy of the thermo-mechanical properties of the crystals. FEA simulations are carried out with the LASCAD software.

The parameters needed for the FEA simulations are the crystal geometry, the fractional thermal load η_h, the absorption coefficient α_{NS}, the pump characteristics, and the geometry of the cooling system. The thermal conductivities values on the crystal axes perpendicular to the pump axis, K_{cx} and K_{cy}, are the fit parameters. The result of the simulation is a complete temperature map of the crystal, and the simulated temperature profiles of the pumped face can be compared to the measurements made with the experimental setup, to find the best fit parameters. Figure 10 presents the optimization process.
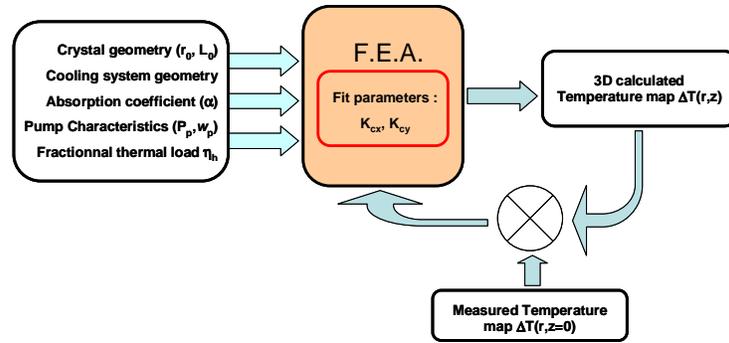
Fig. 10. Principle of the Kc determination by measurements and FEA simulations

The crystal and cooling system geometries are chosen in the FEA program accordingly to the experimental conditions.

The absorption coefficient is considered as constant and measured experimentally [thanks to Eq. (8)]. We checked by calculations with formula (4) that the bleaching effect disappeared in laser operation with all the crystals used for the experiments.

The pump power is chosen accordingly to the experimental measurement, and the pump profile used for the simulation is the supergaussian fit function presented in Fig. 6.

The fractional thermal load is calculated like described in section 2, by formula (11). We calculated the values of the laser extraction efficiency in all cases to be sure that formula (11) is valid.

For an a-cut uniaxial crystal, for example, it is possible to deduce both thermal conductivities in the a and c axes by fitting the simulated and measured experimental temperature profiles in both directions. This can be done on the same temperature map, so both values are obtained exactly in the same experimental conditions.

The crystals are simulated by approximately 90.000 basics elements. The mechanical parameters of the crystal come from tabulated values. We used two sets of Nd:YVO$_4$ and Nd:GdVO$_4$ crystals : 0.1% at. doped, 3x3x10 mm^3 crystals, and 1% at. doped, 3x3x5 mm^3 crystals. All crystals come from CASIX inc.. They are a-cut and one face received HR coating at 1064 nm and anti-reflection (AR) coating at 808 nm. The experimental setup is similar to the one presented in Fig. 5, but the mirror M1 is directly deposed on the crystal face, and a polarizer was inserted in the collimated pump beam to pump the crystal on the pi polarization, corresponding to the c-axis of the crystal.

a) Experiments with 0.1% at. doped crystals

The incident pump power is 23 W on the pi polarization, imaged in a 340 µm diameter spot near the input face of the crystal. The absorption coefficients and resulting $\alpha.P_0$ parameters are summarized in table 1. The laser cavity is composed of the HR coated face of the crystal and a concave mirror M2 with a radius of curvature of 150 mm. With a 15% output coupler, under a pump power of 23W, we achieved a power of 12.3W of laser in the Nd:YVO4 crystal and 11 W in the Nd:GdVO4 crystal in order to check their good laser quality. For all thermal measurements, we used a high reflectivity mirror to increase the intracavity laser power and reach the condition $\eta_l = 1$. (cf. Section 2). The threshold of the laser effect is smaller than 1 W of pump power. The cavity length is adjusted to around L = 80 mm in order to achieve single-spatial mode laser emission. The intracavity laser power is evaluated to 250 W with the Nd:GdVO$_4$ crystals and 300 W with the Nd:YVO$_4$ crystals. The corresponding values of η_l are 0.995 and 0.997, respectively.

Table 1. Incident pump power and absorption coefficients for the 0.1% at. doped crystals.

Crystals	$\alpha\ (cm^{-1})$	$P_o\ (W)$	$\alpha.P_o\ (W/m)$
0.1% Nd:YVO$_4$	1.9	23.2	4408
0.1% Nd:GdVO$_4$	2.3	23.2	5336

The experimental and simulated temperature profiles for a Nd:YVO$_4$ crystal are presented in Fig. 11.
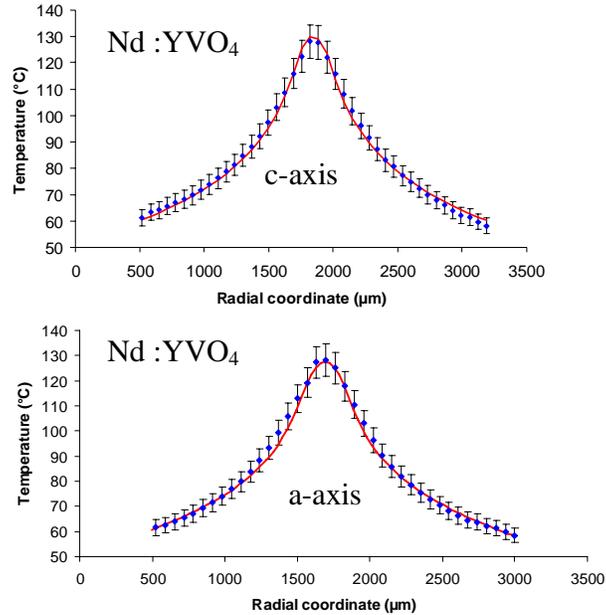

Fig. 11. Experimental (blue) and simulated (red) temperature profiles on the c and a axes of 0.1% at. doped Nd:YVO$_4$ crystal.

The resulting values of the thermal conductivities are summarized in Table 2. Error bars come from calculations made in section 2. Those values are in the range of the different previously published values (Kc between 5 and 11 W/mK for a-cut Nd:YVO$_4$, Kc between 6 and 12 W/mK for a-cut Nd:GdVO$_4$ crystals, along the c-axis), and show a clear advantage for the Nd:GdVO$_4$ crystal compared to Nd:YVO$_4$, which would result in a 20% lower temperature elevation for the same absorbed pump power.

Table 2. Thermal conductivities results for 0.1% at. doped vanadate crystals

Crystals	Kc (c-axis) (W/m.K)	Kc (a-axis) (W/m.K)
0.1% Nd:YVO$_4$	6.6 +/-0.4	5.5 +/-0.3
0.1% Nd:GdVO$_4$	8.0 +/- 0.5	5.6 +/- 0.3

b) Experiments with the 1% at. doped crystals

To test the variation of the thermal conductivity at high doping level, we made measurements with 1% at. doped vanadate crystals. The incident pump power is 10.2 W, imaged in a 440 µm diameter spot near the entrance face of the crystal. This pump power is sufficient to measure with a good precision the temperature differences between the center and the edge of the

crystals, while limiting the risk of damaging them. The absorption coefficients and resulting $\alpha.P_0$ coefficients are summarized in table 3.

Table 3. Incident pump power and absorption coefficients for the 1% at. doped vanadate crystals.

Crystals	α *(cm^{-1})*	P_o *(W)*	$\alpha.P_o$ *(W/m)*
1% Nd:YVO$_4$	6.0	10.1	6060
1% Nd:GdVO$_4$	6.7	10.1	6767

The cavity is adjusted to a length of 85 mm to achieve TEM$_{00}$ emission, and it is closed by a high reflectivity mirror M2 with a radius of curvature of 150 mm.
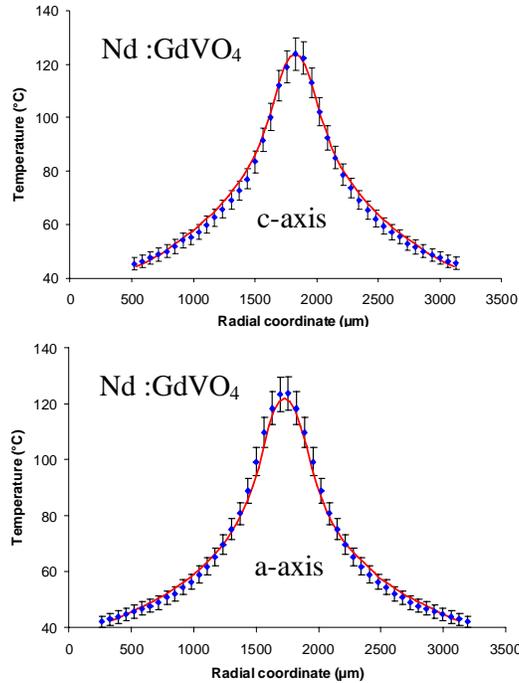

Fig. 12. Experimental (blue) and simulated (red) temperature profiles on the c and a axes of 1% at. doped Nd:GdVO$_4$ crystal.

With a 15% output coupler, under a pump power of 10 W, we achieved 4.5 W of laser in the Nd:YVO4 crystal and 4.2 W in the Nd:GdVO4 crystal, to check their good optical and laser quality. With a high reflectivity mirror, the intracavity power is estimated around 400 W with the Nd:YVO$_4$ crystal, and 350 W with the Nd:GdVO$_4$.This gives η_1 values of 0.996 and 0.994 for the Nd:YVO$_4$ and Nd:GdVO$_4$, respectively. The temperature profiles for a Nd:GdVO$_4$ crystal are shown on Fig. 12. The numerical fit gives values of Kc summarized in Table 4. Those values are very close to the one obtained with 0.1% at. doped crystals.

It is well known that the thermal conductivity is lowered at high doping rates, because of phonon-backscattering in the crystalline lattice. Nevertheless, calculations using the model presented in [18] predict that in Nd:YVO$_4$ the thermal conductivity should only decrease from 6.6 W/(mK) in a 0.1% doped crystal to 6.4 W/(mK) in 1% at. doped crystal. In Nd:GdVO$_4$, the drop off is less noticeable, since the Gadolinium ion have a ionic radius closer to Neodymium than the Yttrium ion : the thermal conductivity should stay very close to 8.0 W/(mK) from 0.1% to 1% at. of Neodymium.

Table 4. Thermal conductivities results for 1% at. doped crystals

Crystals	Kc (c-axis) (W/m.K)	Kc (a-axis) (W/m.K)
1% Nd:YVO$_4$	6.5 +/-0.4	5.5 +/-0.3
1% Nd:GdVO$_4$	8.0 +/- 0.5	5.6 +/- 0.3

The experimental results are in agreement with those calculations, but the precision of the thermal conductivity measurement is not good enough to make quantitative conclusions about such small variations of the conductivity. However, those measurements show that the drop of thermal conductivity for doping concentrations around 1% at. of Neodymium is not significant, especially in Nd:GdVO$_4$. This is in good agreement with previous measurements made by flash method by Ogawa and al. [19]. This also proves that the measurement method is reliable even for highly doped crystals.

We measured a variation of the conductivity between c and a axes of 30% in the Nd:GdVO$_4$ crystals, and 15% in the Nd:YVO$_4$ crystals. Those observations are coherent with the slightly higher anisotropy of the Nd:GdVO$_4$. Previous work reported typical values of 20% of variation between the axes in both crystals [5][11].

6. Discussion and conclusion

We demonstrate a new method of thermal conductivity measurements, by infrared thermography under laser operation. This technique, specific to laser crystals, is an alternative to the usual flash method technique. The determination of the conductivity is direct, with no dependence on thermal diffusivity or specific heat measurements. It is not necessary to depose thin layer of carbon or other material, the laser crystals can be used with their optical coatings. The only thermal information needed to apply formula (12) is the temperature difference observed between the center and the edges of the crystals, and not the absolute maximum temperature measured. In fact, the temperature gradient ΔT is only linked to the absorption and the thermomechanical properties of the crystal, whereas the temperature offset between the copper mount and the edge of the crystal is mainly related to the heat transfer coefficient of the cooling architecture, and the temperature of the copper mount. This is an advantage since the heat transfer coefficients are usually difficult to measure properly. Looking to the IR cartography of the crystal during the measurement is also useful to detect any heat loss or dissymmetry of the heat removal, and avoid false measurements. By using an IR camera working in the 8-12 µm range, in a spectral region where a majority of crystals are strongly absorbant, we avoid direct IR emission through the crystal to the detector. Thanks to that, measurements are not sensible to IR emission coming from the background of the crystal, and there is no integration of the thermal emission along the crystal length. On the other hand, the presented measurement method is limited to good quality crystals, with low concentration of "dead sites" trapping the pump photons or laser photons. Indeed, for low quality crystals, the pump efficiency and the laser efficiency become less than unity and the thermal fraction become higher than the quantum defect, even with high intracavity laser power. In this case, the thermal fraction needs to be measured by another method.

The measurement method is presented here for 4-levels laser transitions, but it can be applied to quasi-3-levels or 3-levels systems by taking into account the saturation of the absorption and the absorption at the laser wavelength. In this case the Eqs. (4) and (10) must be changed accordingly.

For measurements on anisotropic crystals, it is necessary to use a simulation code instead of analytical calculations, and it is then easy to deduce the thermal conductivities of both axes perpendicular to the pump with only one thermal map measurement.

In Nd:YAG crystals, we observed really good agreement between our method and previously published values. This result validates the method and enables us to evaluate the global precision of the method around 6%. In Nd:YVO$_4$ and Nd:GdVO$_4$ crystals, we found thermal

conductivity values inside the range of previously published values. Conductivity of the Nd:GdVO$_4$ crystal was measured to be higher than the one of Nd:YVO$_4$. Those results are in agreement with some previous works [20][7], but in disagreement with the recent systematical study of Saito and Taira [5], who found better conductivity in Nd:YVO$_4$ crystals for doping concentrations below 1% at. in Neodymium. The dispersion of the measurements observed with the flash method and its derivatives can be attributed to several factors, including variations of the quality of the different samples, and experimental issues discussed in the introduction. It is also possible that the heat diffusivity measurement method, using uniform heating on the crystal surface, doesn't really represent the heat conduction properties under pumping and laser conditions, because of the stress induced by the focalization of the pump beam in the crystal. To our knowledge, no study of the variation of the thermal conductivity with the stress conditions has been carried out in laser crystals. If this effect is really important, the new method presented in this work has the advantage to measure the conductivity in operational conditions, under diode-pumping and with laser effect.

Further works will include systematical studies of the crystals on a larger range of doping. We will also add a thermal lens measurement setup, to characterize more completely the thermo-optical properties of laser crystals.

Acknowledgments